

# Stretchable Nanocomposite Sensors, Nanomembrane Interconnectors, and Wireless Electronics toward Feedback–Loop Control of a Soft Earthworm Robot

Riccardo Goldoni,<sup>▽</sup> Yasemin Ozkan-Aydin,<sup>▽</sup> Yun-Soung Kim,<sup>▽</sup> Jongsu Kim, Nathan Zavanelli, Musa Mahmood, Bangyuan Liu, Frank L. Hammond, III, Daniel I. Goldman, and Woon-Hong Yeo\*



Cite This: *ACS Appl. Mater. Interfaces* 2020, 12, 43388–43397



Read Online

ACCESS |



Metrics & More



Article Recommendations



Supporting Information

**ABSTRACT:** Sensors that can detect external stimuli and perceive the surrounding areas could offer an ability for soft biomimetic robots to use the sensory feedback for closed-loop control of locomotion. Although various types of biomimetic robots have been developed, few systems have included integrated stretchable sensors and interconnectors with miniaturized electronics. Here, we introduce a soft, stretchable nanocomposite system with built-in wireless electronics with an aim for feedback–loop motion control of a robotic earthworm. The nanostructured strain sensor, based on a carbon nanomaterial and a low-modulus silicone elastomer, allows for seamless integration with the body of the soft robot that can accommodate large strains caused by bending, stretching, and physical interactions with obstacles. A scalable, cost-effective, and screen-printing method manufactures an array of the strain sensors that are conductive and stretchable over 100% with a gauge factor over 38. An array of nanomembrane interconnectors enables a reliable connection between soft sensors and wireless electronics while tolerating the robot's multimodal movements. A set of computational and experimental studies of soft materials, stretchable mechanics, and hybrid packaging provides the key design factors for a reliable, nanocomposite sensor system. The miniaturized wireless circuit, embedded in the robot joint, offers real-time monitoring of strain changes during the motions of a robotic segment. Collectively, the soft sensor system presented in this work shows great potential to be integrated with other flexible, stretchable electronics for applications in soft robotics, wearable devices, and human-machine interfaces.



**KEYWORDS:** *soft earthworm robot, nanocomposite, stretchable strain sensor, stretchable interconnectors, locomotion, wireless electronics*

## INTRODUCTION

Recent advances in robotics are remarkable and still growing in number due to the continuous innovations in materials science, physics, mechanics, and electronics. The field of soft robotics, in particular, has been the focus of many of these advances. Soft robots are coveted for their natural ability to adapt to environmental uncertainties and compensate for limitations in control and sensing via their mechanical compliance, unlike traditional rigid robots.<sup>1–7</sup> Recent studies have focused on soft robotics inspired by biological systems.<sup>8</sup> For example, a wide variety of living organisms, such as jellyfishes,<sup>9</sup> fishes,<sup>10</sup> octopuses,<sup>11</sup> frogs,<sup>12</sup> salamanders,<sup>13</sup> snakes,<sup>14</sup> rabbits,<sup>15</sup> insects,<sup>16</sup> caterpillars,<sup>17,18</sup> and earthworms<sup>19–23</sup> has inspired the design and fabrication of bioinspired robots. Among those, the study of an earthworm's locomotion has attracted significant interest due to potential applications in environmental exploration and agricultural automation.<sup>24,25</sup> The fundamental principle of movement of every animal is to use their abilities to perceive both the encumbrance of its body (proprioception) and the external environment (exteroception).<sup>26</sup> Rigid robots, made of nondeformable materials, are amenable to proprioception, because rigid mechanical joints regulate their movements with limited degrees of freedom.<sup>27</sup> Conversely, it

is challenging for soft robots, whose deformable bodies include a substantially higher number, nearly infinite, of degrees of freedom.<sup>5</sup> To make soft robots capable of such perception, they must be equipped with soft sensors that can emulate physical sensations felt by humans and animals.<sup>28</sup>

Many different types of soft sensors have been developed, including resistive sensors,<sup>29–32</sup> piezoresistive sensors,<sup>33–36</sup> capacitive sensors,<sup>37,38</sup> and optical sensors.<sup>39–41</sup> There are also plenty of material choices when designing those sensors, including inorganic nanomembranes,<sup>42–44</sup> liquid metals,<sup>29</sup> conductive nanomaterials,<sup>29,45,46</sup> ionic liquids,<sup>30,31</sup> optical fibers,<sup>40,41</sup> or conductive yarns/fabrics.<sup>32,36,38</sup> These sensors are typically encapsulated with silicone elastomers and rubbery materials to fulfill the requirements of elasticity and durability to be suitable for integration with soft robots. A few recent efforts<sup>47–53</sup> have focused on the development of a soft strain

Received: June 11, 2020

Accepted: August 14, 2020

Published: August 14, 2020



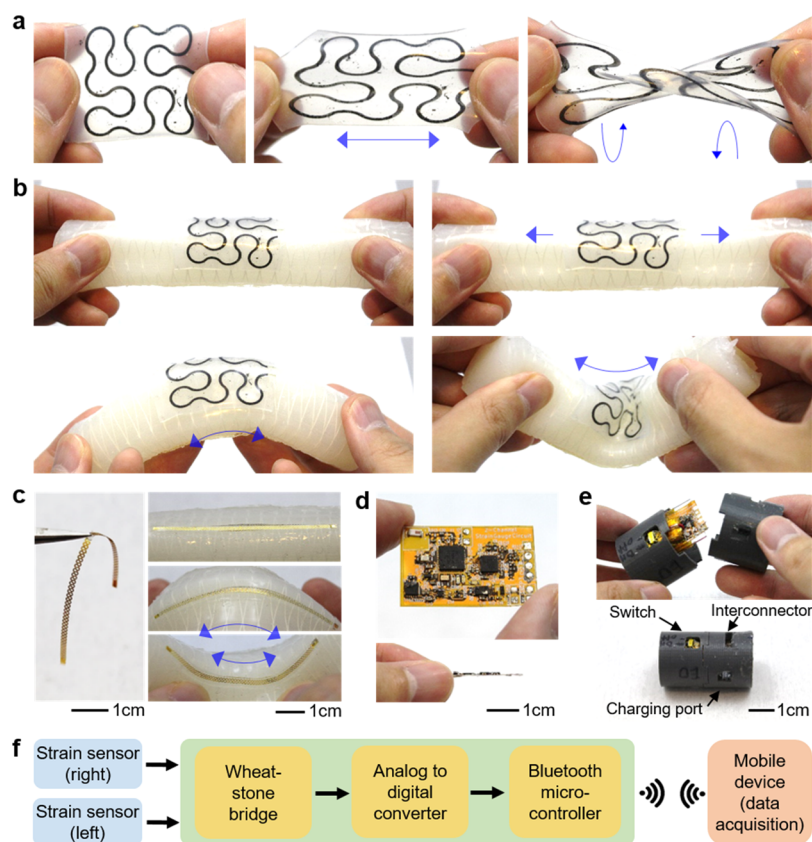


**Figure 1.** Overview of a wireless strain sensing system integrated with a segment of a soft earthworm robot. (a) Nanocomposite strain sensor at unstretched (left), stretched horizontally (middle), and twisted by fingers (right). (b) Sensor-embedded robotic segment at rest (top left), uniaxially stretched (top right), outward bending (bottom left), and inward bending (bottom right). (c) Nanomembrane stretchable interconnectors that can endure multimodal stretching and bending on a soft robotic segment without mechanical fracture. (d) Photos of a miniaturized wireless circuit showing the top view of the entire circuit (top) and side view (bottom). (e) 3D-printed plastic case that incorporates the wireless circuit with dedicated apertures providing physical access. (f) Flowchart showing the signal path from strain sensors to the mobile device.

sensor by using a mixture of nanomaterials and polymers. Although some of the prior works<sup>47–49</sup> show high stretchability and high gauge factors of strain sensors, none of them has demonstrated complete integration of a wireless, soft strain sensor package with a soft robot for a locomotion study. Such a full integration scheme is essential, especially when the soft robot is designed to perform long-range, untethered locomotion, such as conducting a large-area environmental survey or a long-term agricultural soil analysis.

Here, we report a comprehensive study of materials, mechanics, and electronics to develop highly stretchable strain sensors, nanomembrane interconnectors, and miniaturized wireless electronics, together with integrating with a soft robotic earthworm. With the sensor package, this robot can have capabilities of proprioception and exteroception, which enable the control of its deformation and sensing of the surrounding environment. The overall system is mechanically compliant, which facilitates integration with the soft robot. An electronic unit that both acquires and wirelessly transmits the sensor data in real-time is embedded in a 3D-printed rigid segment of the robot and is isolated from the direct effects of internal or external stresses. The highly stretchable and sensitive strain sensors have a potential for various types of applications in soft mobile robotics, flexible wearable systems, and machine interfaces.

## RESULTS AND DISCUSSION

### A Soft Electronic System with Strain Sensors, Stretchable Interconnectors, and Wireless Circuits.

Figure 1 introduces a wireless strain sensing system that incorporates strain sensors, nanomembrane stretchable interconnectors, and wireless electronics. Figure 1a shows the ability of the soft nanocomposite strain sensor that endures mechanical deformations, such as stretching and twisting, without losing structural integrity. The soft robotic segment shown in Figure 1b integrates the soft strain sensors on the surface, which is also stretchable along its length and bendable. We used two types of silicone elastomers to design strain sensors (Ecoflex 0030, Smooth-On) and soft robotic segments (DragonSkin 10, Smooth-On). Such a tight sensor-to-body integration enables accurate and sensitive detection of various actuations performed by the soft segment as well as of external mechanical stimuli presented by the environment. A detailed description of the fabrication of sensors and robotic segments appears in the Supporting Information, Figure S1.

Figure 1c shows thin and stretchable nanomembrane interconnectors that are used to connect strain sensors with a miniaturized printed circuit for wireless data acquisition. The interconnectors are highly bendable and stretchable, providing a compliant deformation mechanism that ensures the integrity and stability of the electrical connection while being embedded on the surface of the soft segment. The thin and flexible circuit

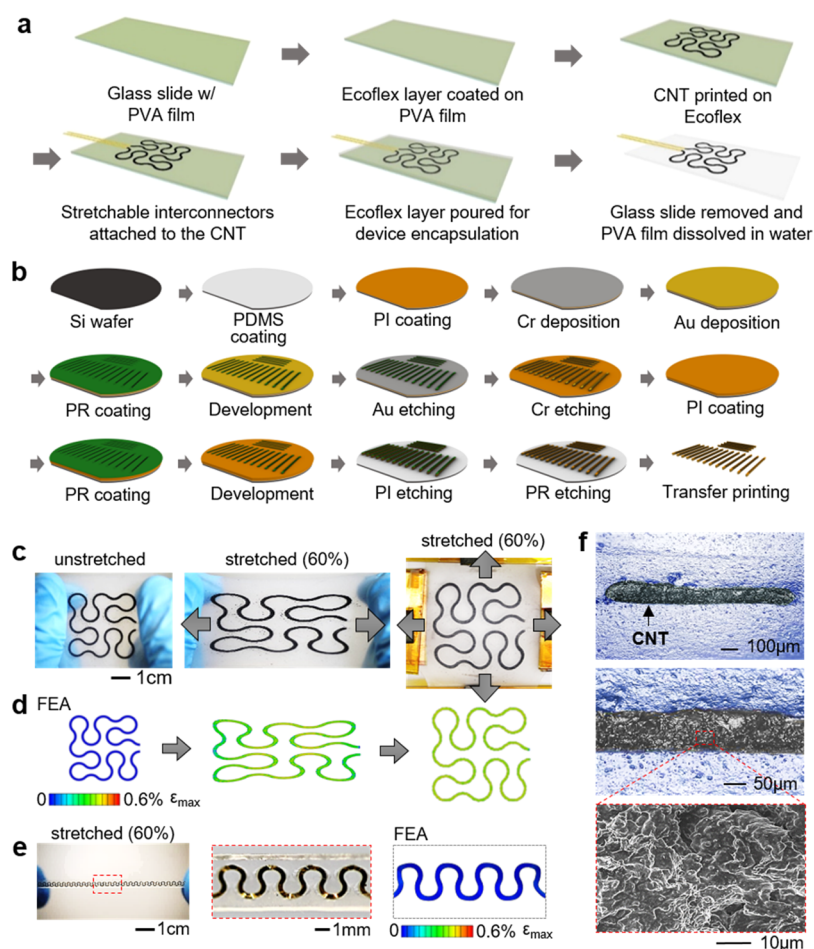


**Figure 2.** Development of a nanocomposite strain sensor and nanomembrane interconnector. (a) Schematic illustration of the fabrication process of a soft strain sensor. (b) Multistep fabrication of stretchable interconnectors. (c) Photos of a fabricated strain sensor at rest (left), 60% uniaxial strain (center), and 60% biaxial strain (right). (d) FEA results, showing the same behavior as the experiment without mechanical fracture. Scale bar: maximum principal strain. (e) Microfabricated stretchable interconnectors with 60% uniaxial strain (left) and with a zoom-in view of the stretched patterns (center) and FEA result showing of the uniaxially stretched interconnector. Scale bar: maximum principal strain. (f) CNT-based strain sensor embedded in a silicone elastomer. Cross-sectional views of microscope images (top and middle) show the CNT trace, while the SEM picture (bottom) captures the densely packed CNT structure.

(Figure 1d) has densely packed chips for seamless integration with a robotic segment. A detailed description of the circuit design and chip components appears in the [Experimental Section](#) and [Supporting Information, Figure S2 and Table S1](#). The wireless electronic unit is inserted into a 3D-printed plastic case to protect it from external stresses during motions of a soft robot. This case is made of two plastic halves that snap-fit together and connects two soft segments. [Figure 1e](#) shows the packaging process along with necessary components, including a switch, battery charging port, and sensor interconnector.

The flowchart in [Figure 1f](#) captures the entire process for the detection of the multimodal segment deformation based on the real-time sensor data. For each wireless electronic circuit, two soft strain sensors are connected, while they detect time-dependent resistance changes caused by segment actuation or exposure to external mechanical stimuli. Based on the Wheatstone bridge configuration, resistance changes in the sensor cause the corresponding changes in voltages measured at the output node of the bridge. The analog voltage data is converted to digital signals by the onboard analog-to-digital converter and is transmitted wirelessly via the Bluetooth Low Energy unit to an external mobile device. Collectively, the

wireless sensor package offers real-time monitoring of strain changes on the surface of a soft robotic segment.

#### Fabrication and Characterization of Nanocomposite Strain Sensors and Nanomembrane Interconnectors.

The fabrication of a soft strain sensor follows a scalable, low-cost method that uses a screen printing technology ([Figure 2a](#)). In this study, we utilized a conductive nanomaterial, carbon nanotubes (CNTs) to design a highly stretchable and sensitive strain sensor. The morphology of nanomaterials that are used as a strain sensing element is a critical factor for maximum stretchability. When embedded in a silicone matrix, nanomaterials in 0D, 1D, and 2D behave differently. According to previous studies,<sup>54,55</sup> strain sensors that use high-aspect-ratio 1D materials (Ag nanowires and CNTs) show better stretchability than sensors with other materials like carbon nanoparticles and graphene.<sup>56–59</sup> For a polymer matrix, we considered both PDMS and Ecoflex and selected Ecoflex due to the enhanced interfacial adhesion with CNTs as demonstrated in the prior work.<sup>60</sup> In this work, multiwalled carbon nanotubes (MWCNT; Nanostructured & Amorphous Materials) and a soft elastomer (Ecoflex) were utilized to offer both conductivity and stretchability. The OH-functionalized

MWCNT was chosen due to its superior compatibility with silicone elastomers to construct nanocomposite sensors.

To provide multiaxial stretchability, the strain sensor has an open-mesh, serpentine pattern (Figure S3). Based on our prior work,<sup>61,62</sup> we have identified optimal parameters to offer stretchability, including a radius of curvature of 270° and a trace width of 1 mm. By using a customized shadow mask, a screen printing method fabricates CNT-embedded elastomeric membranes (details in Figure S4). Afterward, a set of nanomembrane interconnectors are mounted on the sensor's contact pads for electrical connection with a wireless electronic system. Stretchable Ag ink (XE184E, Namics) is dispensed by using a syringe directly onto the contact pads to ensure a firm attachment while providing enough stretchability at the junction. Following the interconnector bonding, the top layer of an elastomer is prepared. The formulation of the top layer is different than that of the bottom layer due to the added cure-retardant component (Slo-Jo, Smooth-On), which allows the top elastomer to fill the voids in the CNT network in the printed trace. Such a process provides a better homogeneity of the sensor while minimizing material dissociation at the interface. Additional details of the fabrication processes appear in the Experimental Section.

The nanomembrane stretchable interconnector is manufactured by following a wafer-based multistep process (Figure 2b), including photolithography, thin film deposition, dry/wet etching, and material transfer printing.<sup>63–65</sup> As illustrated, at the end of a microfabrication process, each wafer produces an array of interconnectors and allows for selective and individual removal of an interconnector during the transfer printing step. The Au nanomembrane is sandwiched by polyimide (PI) to place the core metal into the neutral mechanical plane, which minimizes the bending stress. After the patterning, the interconnector is retrieved from a carrying wafer and then transfer-printed onto the stretchable membrane as prepared for the strain sensor. We conducted a computational mechanics study (finite element analysis; FEA) to estimate the mechanical behavior of both strain sensors and stretchable interconnectors and to avoid undesirable failure from overstretching the components beyond the strain limit of the incorporated materials. Figure 2c shows the top view photographs of a single strain sensor reliably undergoing uniaxial and biaxial stretching up to 60%. Figure 2d describes the results of FEA for the sensor in both deformation states showing the maximum principal strain in both models remains under 1%, indicating the sensor's structural compliance to both uniaxial and biaxial deformations. In the same way, Figure 2e shows the result of 60% uniaxial strain applied to the stretchable interconnector on a soft membrane (thickness: 27 μm), and an inset of a series of four ribbons. Instead of creating locations of high-stress concentration, the individual serpentine pattern allows for the unfolding of the ribbons into more linear curves, which provides reliable and uniform stretchability.

The resulting maximum principal strain below 1% assures reliability for its deformation, considering Au's fracture strain is 1%. Given the maximum expected strain on the sensor and the interconnectors (located on the elongated side) is approximately 15% from the segment bending in 90°, and these FEA results, which used the 60% strain, portray the high and sufficient levels of mechanical stretchability in the sensor and the interconnectors. An optical microscope investigation of the printed sensor (top and middle images; Figure 2f) clearly

captures the Ecoflex-sandwiched CNT structure. An additional image (bottom image; Figure 2f), captured by a scanning electron microscope, shows the successful penetration of Ecoflex inside the CNT trace. Even with a conductive layer coating, the polymer matrix that integrates CNTs accumulates electron charges during SEM imaging, which limits the resolution. However, the SEM micrograph still shows CNT bundles that are well mixed in the polymer.

**Validation of the Performance and Mechanical Reliability of the Sensors.** Figure 3 summarizes the

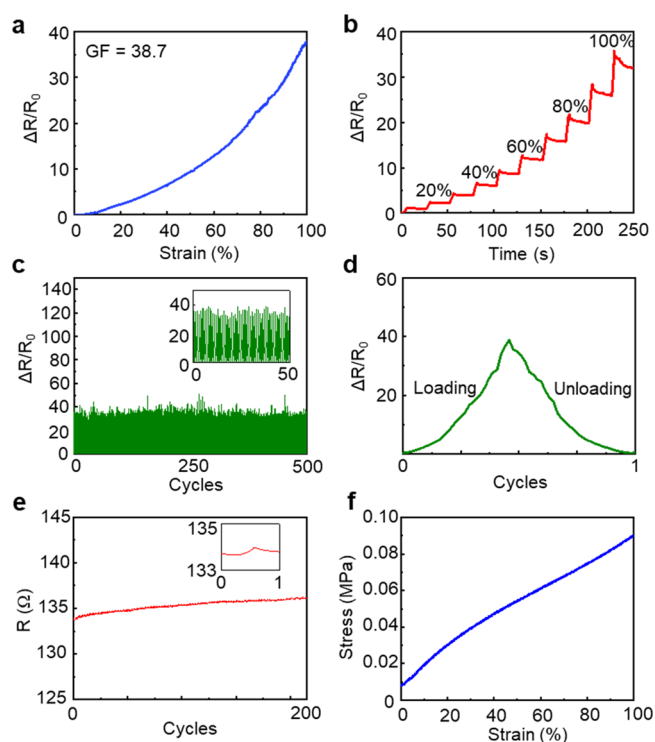


**Figure 3.** Validation of a strain sensor performance. (a) Uniaxial stretching data that measures the resistance change of a strain sensor with applied strain up to 100%. (b) Step stretching test from 0 to 100% (10% strain increase every 20 s) that highlights the relaxation of the elastomeric substrate after stretching. Relaxation is marginal until 80% strain. (c) Uniaxial cyclic stretching test showing consistency of the resistance variation over 500 cycles with 100% tensile strain. Inset shows the data of 50 stretching events. (d) Magnification of a single stretching event from the cyclic stretching test in panel (c), showing symmetric resistance variation in loading and unloading. (e) Uniaxial cyclic test of a nanomembrane stretchable interconnector. Marginal variation in resistance over 200 cycles with 60% tensile strain. Inset shows data of a single stretching event. (f) Stress–strain curve of the interconnector in panel (e) with 100% tensile strain.

performance of a fabricated strain sensor, which includes ultimate stretchability, sensitivity, and reliability during cyclic stretching. A set of uniaxial and cyclic stretching tests was conducted by using a mechanical stretcher and force gauge (ESM303, Mark-10). Details of the experiment setup appear in the Supporting Information Figure S5. The sensitivity of a strain sensor is defined by the gauge factor (GF):<sup>49</sup>

$$GF = \frac{\Delta R/R_0}{\epsilon}$$

where  $\epsilon$  is the engineering strain showing the ratio of the total displacement to the initial dimension,  $\Delta R$  is the relative change in resistance, and  $R_0$  is the initial resistance at  $\epsilon = 0\%$ .

Table 1. Comparison of the Design and Performance of Stretchable Strain Sensors

reference	application	sensor design	material	gauge factor	data acquisition	stretchability (%)
<i>This work</i>	strain detection for guided robotic control	serpentine-patterned sensor	Ecoflex/CNTs	38.7	long-range wireless (Bluetooth)	100
Chong et al. (2019)	monitoring of blood flow	rosette type sensor	PDMS/CB	7.5	wired	50
Jeong et al. (2017)	human motion detection	rosette type sensor	PDMS/GaInSn	2	near-field wireless	50
Gao et al. (2019)	monitoring of human health	strain sensor array	Ecoflex/SiC	250,000	near-field wireless	5
Tang et al. (2019)	plant growth monitoring	linear strain sensor	latex/graphite/CNTs	352	wired	150
Chen et al. (2020)	human motion detection	transparent strain sensor	PDMS/CNTs	14	wired	130
Wang et al. (2018)	human motion detection	rosette type sensor	PDMS/CNTs	35.75	wired	45
Gogurla et al. (2019)	human motion detection	strain sensor in Bio-TENG	silk/AgNWs	30	wired	5
Li et al. (2020)	human motion detection	linear strain sensor	MWCNTs/PDMS microspheres	7.22	wired	40
Lu et al. (2019)	human motion detection	linear strain sensor	MWCNTs/PU	65.7	wired	3
Park et al. (2020)	human motion detection	linear strain sensor	SWCNTs/PDMS	2.75	wired	80
Wang et al. (2019)	human motion detection	linear strain sensor	TPU/CNTs/PDMS	0.339	wired	100
Fu et al. (2019)	human motion detection	linear strain sensor	MWCNTs/PDMS	9	wired	40

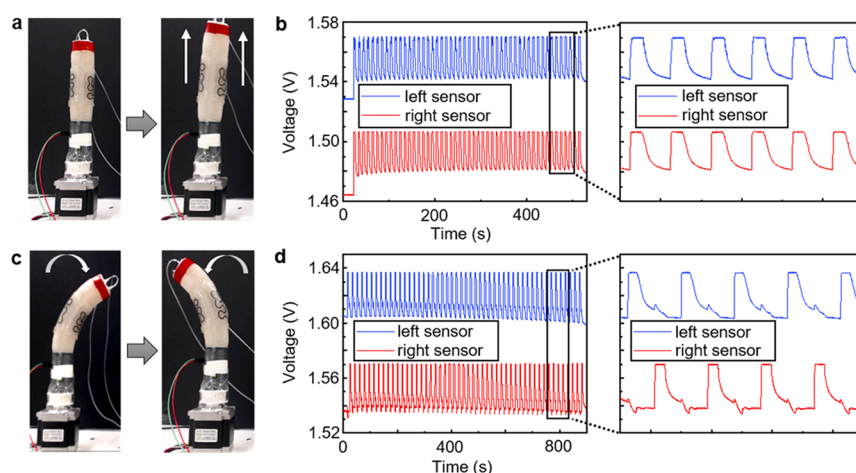


**Figure 4.** Detection of the bending deformation state with a pair of strain sensors. (a) Photos showing forward stretching of a soft robot segment. Two chambers of the segment are inflated by the applied pressure ( $\sim 15$  psi). (b) Voltage changes measured by two strain sensors during the cyclic forward stretching of the robot in panel (a). Magnified graph on the right shows measured voltage peaks for 60 s. (c) Photos of the robot segment undergoing left and right bending. (d) Cyclic bending data measured by a pair of strain sensors on the robot surface. Magnified graph on the right shows 100 second, out-of-phase voltage peaks.

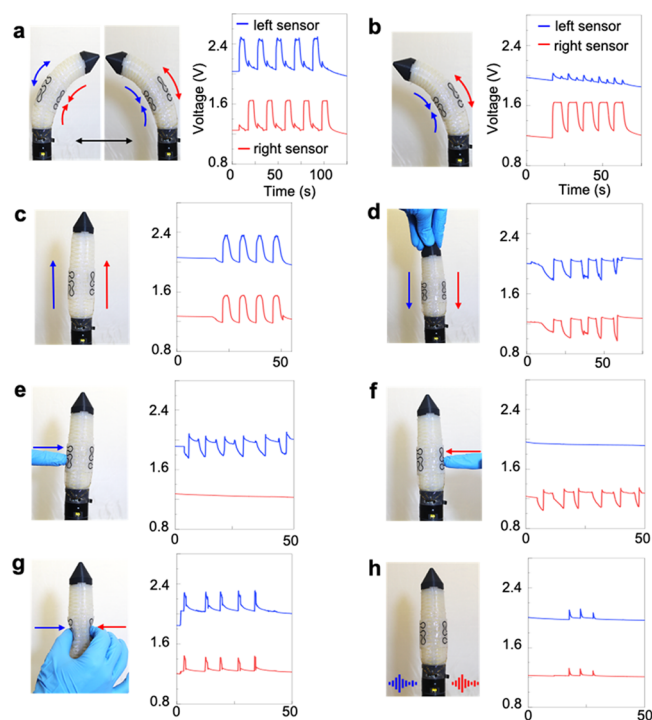
Figure 3a summarizes the sensitivity ( $GF = 38.7$ ) of the fabricated strain sensor. The curve highlights a trend closely fitting an exponential fashion with a value of  $R^2 = 0.996$ . Figure 3b shows the data of time-dependent changes of the sensor response when stretched up to 100%. In the experiment, the sensor was held at a fixed strain for 20 s following 10% stretching. Our sensor showed excellent stability in terms of resistance (relative resistance changes less than 6%) when kept at a constant strain until  $\epsilon \sim 80\%$ . To validate the sensor's reliability, a cyclic stretching test from 0 to 100% uniaxial strain has been performed up to 500 cycles. Figure 3c shows how the strain sensor maintains its sensitivity throughout the whole experiment showing marginal drift in the value of  $\Delta R/R_0$  at  $\epsilon = 100\%$ . The inset shows a detailed view of 50 cycles. The peaks relative to each of the 500 cycles have been identified, resulting in an average  $GF = 34.6$  with a standard deviation  $\sigma = 2.2$ .

Figure 3d captures the behavior of the soft strain sensor in both loading and unloading conditions. Typically, a silicone substrate has a long relaxation time when strain is applied. As a result, the relative resistance change during loading and unloading shows an asymmetric relationship. However, the soft sensor in Figure 3d shows a symmetric behavior in the loading and unloading conditions. It was found out that the deformation speed played a key role in governing the relaxation effect. In the tensile stretching tests, we used two different speeds: 50 for Figure 3b and 200 mm/min for Figure 3c,d. While Figure 3b shows a typical viscoelastic behavior of the elastomer-embedded sensor at a strain higher than 80% with fast-speed deformation at a speed of 200 mm/min, the strain sensor in Figure 2d shows a nearly symmetrical behavior of the resistance change during loading–unloading cycles. With short deformation time, the CNTs in the nanocomposite were minimally influenced by the rearrangement effect of

CNTs in the silicone matrix. In addition, Figure 3e summarizes the result of cyclic stretching of a fabricated nanomembrane interconnector with 200 cycles from 0 to 60% strain. The result shows negligible resistance change ( $\Delta R/R_0 = 0.02$ ), compared to that from the strain sensor ( $\Delta R/R_0 = 40$ ). Figure 3f captures the stress change of the interconnector according to the increased strain up to 100%. Collectively, Table 1 compares the design and performance of the strain sensor in this study with published works,<sup>47–53,66–70</sup> which captures the main contribution of our work that reports a fully integrated wireless sensor system for a soft robot application. The measured experimental data were used to accurately model our strain sensor for the FEA simulations. In the computational study, the Ogden function<sup>71</sup> for energy potential was used to study large deformations in soft sensors and soft robotic motions.

**Quantification of the Deformation of a Soft Robotic Segment.** Figure 4 summarizes a quantitative detection and analysis of a soft robot's deformation via surface-embedded, soft strain sensors. The main goal of this study is to demonstrate the sensor's ability to detect the encumbrance of the robot body (proprioception) and to perceive the surrounding environment and adjacent objects (exteroception). As shown in Figure 4a,b, when the soft segment performs forward stretching (40%), both left and right strain sensors respond simultaneously to the internal stimulus. In addition, the strain sensor can monitor the segment's cyclic bending in different directions (maximum bending: 60°). In the experimental study, the segment's base was completely fixed to a metal plate to ensure stability during the deformation test. We used a pneumatic controller to inflate the soft robotic segment with an internal pressure of 15 psi. Figure 4a captures photos of a soft robotic segment that is elongated vertically due to the applied pressure. The magnified data set in Figure 4b shows identical voltage peaks on the two curves, capturing an accurate response from two strain sensors on the simultaneous elongation of the soft segment. Figure 4c shows photos of a cyclic bending test of the soft robotic segment that undergoes repeated bending to the right and to the left (over 50 times). The measured data in Figure 4d clearly captures that two sensors can detect the bending deformation in different directions. While the voltage peaks ( $\Delta V = \sim 400$  mV) are consistent with the forward stretching case, left and right bending cases show out-of-phase signals. Whenever one sensor undergoes stretching, the opposite sensor produces a small voltage drop ( $\Delta V = \sim 40$  mV), associated with its corresponding compression. The details of the real-time actuation of the soft robotic segment and wireless acquisition of strain sensor data appear in Supporting Video S1 and Video S2.

**Proficiency of Soft Nanomembrane Sensors in the Robot's Proprioception and Exteroception.** Figure 5 represents a set of experimental studies that capture the soft sensor's capabilities in proprioception and exteroception caused by internal and external stimuli to a soft robot. A pair of stretchable strain sensors is mounted on the surface of a robotic segment by using Ecoflex as a glue to enhance the adhesion. No relative dissociation or delamination between the parts was observed during the mechanical tests and other actuation experiments. Figure 5a shows a sequence of alternating voltage peaks that are caused by the alternative right and left bending motions of the segment. Figure 5b is associated with a repetition of left bending, aiming to generate voltage signals associated with being repeatedly compressed by



**Figure 5.** Proficiency of soft robot-embedded nanomembrane sensors in proprioception and exteroception. Series of photos and corresponding graphs show various types of robot actuation and measured data by two sensors and wireless electronics. Soft robot segment undergoes the following motions: (a) alternating left and right bending, (b) repeated left bending, (c) actuated elongation, (d) vertical compression, (e) tactile sensing on the left side, (f) tactile sensing on the right side, (g) simultaneous lateral compression, and (h) simulated ground vibration.

the bending motion of the segment (e.g., the left sensor). For the demonstration of exteroception, we applied external pressure to the soft robotic segment. When the robot segment is elongated (Figure 5c), two soft sensors show sharp peaks in the measured voltages. Afterward, the robot segment is compressed by applying a downward force to the terminal end (Figure 5d), which mimics a situation where the motion of the segment is impeded by a rigid object. Figure 5e,f shows the responses of two sensors when external directional forces are applied. In Figure 5e, the left side of the robot segment is repeatedly pushed by a finger while Figure 5f shows the applied force to the right side of the segment. Two sensors that are mounted on the segment's surface clearly detect the directional forces and amounts. When forces are applied simultaneously (Figure 5g), then two sensors show identical changes in the voltage measurement. Figure 5h mimics an environmental noise that an earthworm robot may experience in the soil. The gentle tapping of the segment's base plate causes ground vibration. Two sensors can successfully detect the small voltage changes ( $\sim 100$  mV). Overall, the sensor-embedded robot segment demonstrates its capability to detect both internal and external stimuli, which mimic realistic situations that an earthworm robot will experience. Based on this study, our future work will focus on automatic detection and classification of external stimuli toward feedback-loop control of a soft earthworm robot.

**Application of the Wireless Strain Sensing System for Integration with a Soft Robotic Earthworm.** Figure 6 shows a possible application of the newly developed strain

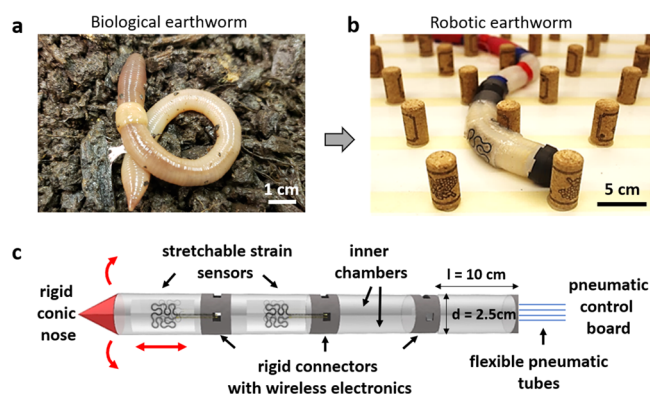


**Figure 6.** Application of the wireless strain sensing system for a soft earthworm robot. (a) Photo of an earthworm (*Lumbricus terrestris*) that has a long, flexible, segmented, and hydrostatic skeleton. (b) Soft robotic earthworm moving through a heterogeneous environment. (c) Schematic illustration of the robot, including embedded two pairs of strain sensors, miniaturized wireless electronics in a 3D-printed custom connector, and soft tubing for pneumatic actuation of the robot. Each segment has two inner chambers, which allows the segment to bend left and right and extend longitudinally (indicated by red arrows).

sensing system for full integration with a soft earthworm robot. Earthworms (*Lumbricus terrestris*) have segmented, hydrostatic skeletons and during crawling and burial can use a peristaltic gait defined by the elongation and contraction of longitudinal and circular muscles around the body in sequence.<sup>72</sup> We designed a soft earthworm robot using the most widely used pneumatic elastomer actuators to model the shape and basic behavior of natural earthworms living in a heterogeneous environment (Figure 6a). Based on an elastomeric construction,<sup>73</sup> the soft robot (Figure 6b) is constructed by connecting fiber-reinforced soft pneumatic actuators presented in the previous section in series. Each actuator has two half-cylinder inner chambers ( $r = 12.5$  mm) that are made of two concentric layers of elastomer with Kevlar threads between as reinforcement. As described earlier, each actuator is capable of bending and elongating depending on the pressure difference of its two inner chambers. Details of the fabrication process and the structural description of the robotic worm appear in the Experimental Section and Figure S1. Between each actuator, there are 3D-printed plastic cases that serve as both the mechanical joints and environmental shield for the wireless electronics. The printed case has two apertures: one for the stretchable interconnectors connecting strain sensors with the circuit and the other for the connection of a rechargeable battery. Figure 6c illustrates the details of the robot that shows the integration of multiple soft segments, strain sensors, and wireless electronics. The system allows the integration of numerous segments to replicate the movement of worms of different sizes. However, to simplify the design and control system in this work, we built the robot with four segments: two for anchoring (bending segments at the front and back) and two for elongation (middle segments). In this study, we used the pneumatic actuation to control the soft earthworm robot due to the high power density and resilience. The elastomer-based actuators mimic the shapes and behavior of real earthworms. Overall, this study shows the feasibility of successful integration of stretchable sensors and wireless electronics with a soft robot. The ultimate goal of this study is to use multiple soft sensors for the detection of pressure

changes from the mechanical interaction of the robot with its surrounding. The robot will then use this feedback for closed-loop control of locomotion to utilize or avoid obstacles, such as the ground and the rocks. Such feedback can also allow the robot to modulate and optimize its gait according to its environment.

## CONCLUSIONS

In this paper, we introduce a newly developed soft electronic system, including an array of nanocomposite strain sensors, stretchable interconnectors, and wireless electronics, which is seamlessly integrated into the body of a soft robotic segment for detection of its deformation. The high elasticity of the CNT-based nanocomposite, employed in the sensor fabrication, guarantees excellent compliance for the whole range of movements (bending and stretching) that the robot could perform. Moreover, the high sensitivity of CNT-enabled strain sensors makes this system suitable for multimodal tactile sensing. The wireless electronic system that incorporates soft sensors shows the potential for other applications that require remote monitoring and obstacle detection with untethered robots. Future work will focus on the study of precise pneumatic control and feedback-loop control of a soft earthworm robot in realistic soil environments.

## EXPERIMENTAL SECTION

**Fabrication of a Nanocomposite Strain Sensor.** The strain sensor consists of a screen-printed serpentine trace of multiwalled carbon nanotubes (Nanostructured & Amorphous Materials) sandwiched between two layers of a silicone elastomer (Ecoflex 0030, Smooth-On). OH-functionalized CNTs have been chosen among other types of functionalization due to their good compatibility with elastomer matrices. The first layer of a silicone substrate is poured on a glass slide coated with polyvinyl alcohol (PVA) film and let cure. The CNTs are deposited through a shadow mask that is prepared by a femtosecond laser micromachining system (Optec WS-Flex). Microfabricated stretchable interconnectors are joined to the leads of the CNT-printed trace by using stretchable silver ink (XE184E, Namics). The microfabrication of stretchable interconnectors uses a PDMS-coated silicon wafer as a handle substrate. On top of the PDMS layer, layers of PI and Cr/Au are deposited and patterned through metallization, photolithography, and etching. After the patterning, we utilize a water soluble tape to selectively retrieve each interconnector from the wafer to transfer print on a soft elastomer (Ecoflex) for subsequent encapsulation and integration with a robotic segment. More details of the microfabrication of strain sensors and stretchable interconnectors are provided in the Supporting Information Note S1. Following the ink curing process, the second layer of silicone is poured for encapsulation of the device and let cure. The entire device is then cut out and peeled off from the underlying PVA film.

**Fabrication of a Wireless Electronic Circuit.** The data acquisition system for the strain sensor includes a Bluetooth Low Energy microcontroller (nRF52832, Nordic Semiconductor) integrated with a two-channel 24-bit analog-to-digital converter front end (ADS1292, Texas Instruments), with the inputs configured as a Wheatstone bridge. The system is powered by a rechargeable lithium polymer battery (3.7 V). The front end chip simultaneously samples at 125 samples per second on both channels, and the data are transmitted wirelessly to an Android tablet, where the data are plotted, recorded, and analyzed. The wireless transmission latency is about 20 ms. The Bluetooth module is capable of maintaining a robust wireless connection with the tablet for up to 20 m. A complete list of electronic components used for the wireless circuit is shown in Table S1.

**Fabrication of a Soft Earthworm Robot.** The soft earthworm robot is assembled using four repetitive, 140 mm-long soft segments.

Each segment contains two subchambers, which are cast with DragonSkin10 NV silicone (Smooth-On) in 3D-printed molds (uPrint SE Plus, Stratasys, Ltd.). Once the inner layer is cured, the Kevlar thread is wrapped around the semicylindrically shaped inner skin of the subchamber to constrain the radial expansion. The outer layer is cast in a bigger mold to fix the threads and relative position of two subchambers. After removing the 3D-printed semicylindrically shaped inner bar and sealing the top and bottom of the two subchambers, the fabrication of the single bending segment is finished. An illustrative description of the fabrication process is shown in Figure S1.

## ■ ASSOCIATED CONTENT

### SI Supporting Information

The Supporting Information is available free of charge at <https://pubs.acs.org/doi/10.1021/acsami.0c10672>.

Fabrication of nanocomposite sensors and electronics (Note S1); fabrication process and structural description of a soft robotic segment (Figure S1); design of a flexible circuit (Figure S2); designs for sensors and interconnectors (Figure S3); experimental setup for screen printing (Figure S4); experimental setup for uniaxial stretching (Figure S5); list of electronic components for a printed circuit board (Table S1) (PDF)

Evaluation of the sensor system via a cyclic forward stretching test (Video S1) (MP4)

Evaluation of the sensor system via a cyclic bending test (Video S2) (MP4)

## ■ AUTHOR INFORMATION

### Corresponding Author

**Woon-Hong Yeo** – *George W. Woodruff School of Mechanical Engineering, Institute for Electronics and Nanotechnology and Parker H. Petit Institute for Bioengineering and Biosciences, Neural Engineering Center, Institute for Materials, Institute for Robotics and Intelligent Machines, Georgia Institute of Technology, Atlanta, Georgia 30332, United States; Wallace H. Coulter Department of Biomedical Engineering, Atlanta, Georgia 30332, United States; [orcid.org/0000-0002-5526-3882](https://orcid.org/0000-0002-5526-3882); Email: [whyeo@gatech.edu](mailto:whyeo@gatech.edu)*

### Authors

**Riccardo Goldoni** – *George W. Woodruff School of Mechanical Engineering, Institute for Electronics and Nanotechnology and School of Materials Science and Engineering, Georgia Institute of Technology, Atlanta, Georgia 30332, United States*

**Yasemin Ozkan-Aydin** – *School of Physics, Georgia Institute of Technology, Atlanta, Georgia 30332, United States*

**Yun-Soung Kim** – *George W. Woodruff School of Mechanical Engineering, Institute for Electronics and Nanotechnology, Georgia Institute of Technology, Atlanta, Georgia 30332, United States*

**Jongsu Kim** – *George W. Woodruff School of Mechanical Engineering, Institute for Electronics and Nanotechnology, Georgia Institute of Technology, Atlanta, Georgia 30332, United States*

**Nathan Zavanelli** – *George W. Woodruff School of Mechanical Engineering, Institute for Electronics and Nanotechnology and School of Electrical and Computer Engineering, Georgia Institute of Technology, Atlanta, Georgia 30332, United States*

**Musa Mahmood** – *George W. Woodruff School of Mechanical Engineering, Institute for Electronics and Nanotechnology, Georgia Institute of Technology, Atlanta, Georgia 30332, United States*

**Bangyuan Liu** – *George W. Woodruff School of Mechanical Engineering, Georgia Institute of Technology, Atlanta, Georgia 30332, United States*

**Frank L. Hammond, III** – *George W. Woodruff School of Mechanical Engineering, Georgia Institute of Technology, Atlanta, Georgia 30332, United States; Wallace H. Coulter Department of Biomedical Engineering, Atlanta, Georgia 30332, United States*

**Daniel I. Goldman** – *School of Physics, Georgia Institute of Technology, Atlanta, Georgia 30332, United States*

Complete contact information is available at: <https://pubs.acs.org/doi/10.1021/acsami.0c10672>

### Author Contributions

<sup>▽</sup>These authors contributed equally.

### Author Contributions

R.G., Y.-S.K., and W.-H.Y. conceived and designed the research; R.G., Y.O.A., Y.-S.K., J.K., N.Z., and B.L. performed the experiments; R.G., Y.-S.K., and J.K. fabricated the sensors and electronics; Y.O.A. and B.L. fabricated the worms; and Y.O.A. conducted robot actuation tests. R.G., Y.-S.K., and Y.O.A. analyzed the data; M.M. designed the electronics and the data acquisition software; F.L.H. and D.I.G. provided guidance on the robot study; and R.G., Y.O.A., Y.-S.K., and W.-H.Y. wrote the paper.

### Notes

The authors declare no competing financial interest.

## ■ ACKNOWLEDGMENTS

W.-H.Y. acknowledges the support from the NextFlex-Department of Defense, the National Science Foundation (1939094), and the Institute for Electronics and Nanotechnology, and a member of the National Nanotechnology Coordinated Infrastructure, which is supported by the National Science Foundation (grant no. ECCS-1542174). The authors acknowledge the 2017 Georgia Tech IRIM Seed Grant that supported early research on the soft earthworm robot.

## ■ REFERENCES

- (1) Yang, G.-Z.; Bellingham, J.; Dupont, P. E.; Fischer, P.; Floridi, L.; Full, R.; Jacobstein, N.; Kumar, V.; McNutt, M.; Merrifield, R.; Nelson, B. J.; Scassellati, B.; Taddeo, M.; Taylor, R.; Veloso, M.; Wang, Z. L.; Wood, R. The Grand Challenges of Science Robotics. *Sci. Robot.* **2018**, *3*, eaar7650.
- (2) Bauer, S.; Bauer-Gogonea, S.; Graz, I.; Kaltenbrunner, M.; Keplinger, C.; Schwödiauer, R. 25th Anniversary Article: A Soft Future: From Robots and Sensor Skin to Energy Harvesters. *Adv. Mater.* **2014**, *26*, 149–162.
- (3) Rus, D.; Tolley, M. T. Design, Fabrication and Control of Soft Robots. *Nature* **2015**, *521*, 467–475.
- (4) Calisti, M.; Picardi, G.; Laschi, C. Fundamentals of Soft Robot Locomotion. *J. R. Soc., Interface* **2017**, *14*, 20170101.
- (5) Iida, F.; Laschi, C. Soft Robotics: Challenges and Perspectives. *Procedia Comput. Sci.* **2011**, *7*, 99–102.
- (6) Trimmer, B. Soft Robots. *Curr. Biol.* **2013**, *23*, R639–R641.
- (7) Majidi, C. Soft Robotics: A Perspective - Current Trends and Prospects for the Future. *Soft Robot.* **2014**, *1*, 5–11.
- (8) Kim, S.; Laschi, C.; Trimmer, B. Soft Robotics: A Bioinspired Evolution in Robotics. *Trends Biotechnol.* **2013**, *31*, 287–294.
- (9) Yeom, S.-W.; Oh, I.-K. A Biomimetic Jellyfish Robot Based on Ionic Polymer Metal Composite Actuators. *Smart Mater. Struct.* **2009**, *18*, No. 085002.
- (10) Porez, M.; Boyer, F.; Ijspeert, A. J. Improved Lighthill Fish Swimming Model for Bio-Inspired Robots: Modeling, Computational

Aspects and Experimental Comparisons. *Int. J. Rob. Res.* **2014**, *33*, 1322–1341.

(11) Calisti, M.; Arienti, A.; Renda, F.; Levy, G.; Hochner, B.; Mazzolai, B.; Dario, P.; Laschi, C. Design and Development of a Soft Robot With Crawling and Grasping Capabilities. In *2012 IEEE International Conference on Robotics and Automation*; IEEE: 2012; 4950–4955.

(12) Su, K. Y.; Gul, J. Z.; Choi, K. H. A Biomimetic Jumping Locomotion of Functionally Graded Frog Soft Robot. In *2017 14th International Conference on Ubiquitous Robots and Ambient Intelligence (URAI)*; IEEE: 2017.

(13) Ijspeert, A. J.; Crespi, A.; Cabelguen, J.-M. Simulation and Robotics Studies of Salamander Locomotion. *Neuroinformatics* **2005**, *3*, 171–196.

(14) Luo, M.; Pan, Y.; Skorina, E. H.; Tao, W.; Chen, F.; Ozel, S.; Onal, C. D. Slithering Towards Autonomy: A Self-contained Soft Robotic Snake Platform With Integrated Curvature Sensing. *Bioinspiration Biomimetics* **2015**, *10*, No. 055001.

(15) Oshima, T.; Momose, N.; Koyanagi, K.; Matsuno, T.; Fujikawa, T. Jumping Mechanism Imitating Vertebrate by the Mechanical Function of Bi-Articular Muscle. In *2007 International Conference on Mechatronics and Automation*; IEEE: 2007; 1920–1925.

(16) Li, F.; Liu, W.; Fu, X.; Bonsignori, G.; Scarfogliero, U.; Stefanini, C.; Dario, P. Jumping Like an Insect: Design and Dynamic Optimization of a Jumping Mini Robot Based on Bio-Mimetic Inspiration. *Mechatronics* **2012**, *22*, 167–176.

(17) Umedachi, T.; Vikas, V.; Trimmer, B. A. Highly Deformable 3-D Printed Soft Robot Generating Inching and Crawling Locomotions With Variable Friction Legs. In *2013 IEEE/RSJ International Conference on Intelligent Robots and Systems*; IEEE: 2013; 4590–4595.

(18) Trimmer, B.; Takesian, A.; Sweet, B.; Rogers, C.; Hake, D.; Rogers, D. Caterpillar Locomotion: A New Model for Soft-Bodied Climbing and Burrowing Robots. In *Proceedings of the 7th International Symposium on Technology and the Mine Problem*; 2006.

(19) Daltorio, K. A.; Boxerbaum, A. S.; Horchler, A. D.; Shaw, K. M.; Chiel, H. J.; Quinn, R. D. Efficient Worm-Like Locomotion: Slip and Control of Soft-bodied Peristaltic Robots. *Bioinspiration Biomimetics* **2013**, *8*, No. 035003.

(20) Kim, B.; Lee, M. G.; Lee, Y. P.; Kim, Y.; Lee, G. An Earthworm-Like Micro Robot Using Shape Memory Alloy Actuator. *Sens. Actuators, A* **2006**, *125*, 429–437.

(21) Seok, S.; Onal, C. D.; Cho, K.-J.; Wood, R. J.; Rus, D.; Kim, S. Meshworm: A Peristaltic Soft Robot With Antagonistic Nickel Titanium Coil Actuators. *IEEE/ASME Trans Mechatron.* **2013**, *18*, 1485–1497.

(22) Nakamura, T.; Iwanaga, T. In Locomotion Strategy for a Peristaltic Crawling Robot in a 2-Dimensional Space. In *2008 IEEE International Conference on Robotics and Automation*; IEEE: 2008; 238–243.

(23) Menciassi, A.; Gorini, S.; Pernorio, G.; Dario, P. A SMA Actuated Artificial Earthworm. In *IEEE International Conference on Robotics and Automation, 2004. Proceedings. ICRA'04. 2004*; IEEE: 2004; 3282–3287.

(24) Methenitis, G.; Hennes, D.; Izzo, D.; Visser, A. Novelty Search for Soft Robotic Space Exploration. In *Proceedings of the 2015 Annual Conference on Genetic and Evolutionary Computation*; 2015; 193–200.

(25) Liu, B.; Ozkan-Aydin, Y.; Goldman, D. I.; Hammond, F. L. Kirigami Skin Improves Soft Earthworm Robot Anchoring and Locomotion Under Cohesive Soil. In *2019 2nd IEEE International Conference on Soft Robotics (RoboSoft)*; IEEE: 2019; 828–833.

(26) Soter, G.; Conn, A.; Hauser, H.; Rossiter, J. Bodily Aware Soft Robots: Integration of Proprioceptive and Exteroceptive Sensors. In *2018 IEEE International Conference on Robotics and Automation (ICRA)*; IEEE: 2018; 2448–2453.

(27) Laschi, C.; Cianchetti, M.; Mazzolai, B.; Margheri, L.; Follador, M.; Dario, P. Soft Robot Arm Inspired by the Octopus. *Adv. Robot.* **2012**, *26*, 709–727.

(28) Pfeifer, R.; Lungarella, M.; Iida, F. The Challenges Ahead for Bio-Inspired ‘Soft’ Robotics. *Commun. ACM* **2012**, *55*, 76–87.

(29) Morrow, J.; Shin, H.-S.; Phillips-Grafflin, C.; Jang, S.-H.; Torrey, J.; Larkins, R.; Dang, S.; Park, Y.-L.; Berenson, D. Improving Soft Pneumatic Actuator Fingers Through Integration of Soft Sensors, Position and Force control, and Rigid Fingernails. In *2016 IEEE International Conference on Robotics and Automation (ICRA)*; IEEE: 2016; 5024–5031.

(30) Noda, K.; Iwase, E.; Matsumoto, K.; Shimoyama, I. Stretchable Liquid Tactile Sensor for Robot-Joints. In *2010 IEEE International Conference on Robotics and Automation*; IEEE: 2010; 4212–4217.

(31) Helps, T.; Rossiter, J. Proprioceptive Flexible Fluidic Actuators Using Conductive Working Fluids. *Soft Robot* **2018**, *5*, 175–189.

(32) Wurdemann, H. A.; Sareh, S.; Shafti, A.; Noh, Y.; Faragasso, A.; Chaturanga, D. S.; Liu, H.; Hirai, S.; Althoefer, K. Embedded Electro-Conductive Yarn for Shape Sensing of Soft Robotic Manipulators. In *2015 37th Annual International Conference of the IEEE Engineering in Medicine and Biology Society (EMBC)*, IEEE: 2015; 8026–8029.

(33) Kure, K.; Kanda, T.; Suzumori, K.; Wakimoto, S. Flexible Displacement Sensor Using Injected Conductive Paste. *Sens. Actuators, A* **2008**, *143*, 272–278.

(34) Kuriyama, S.; Ding, M.; Kurita, Y.; Ueda, J.; Ogasawara, T. Flexible Sensor for McKibben Pneumatic Artificial Muscle Actuator. *Int. J. Autom. Technol.* **2009**, *3*, 731–740.

(35) Koivikko, A.; Raei, E. S.; Mosallaei, M.; Mäntyselä, M.; Sariola, V. Screen-Printed Curvature Sensors for Soft Robots. *IEEE Sens. J.* **2017**, *18*, 223–230.

(36) Khin, P.; Low, J.; Lee, W.; Kukreja, S. L.; Ren, H.; Thakor, N. V.; Yeow, C.-H. Soft Haptics Using Soft Actuator and Soft Sensor. In *2016 6th IEEE International Conference on Biomedical Robotics and Biomechatronics (BioRob)*; IEEE: 2016; 1272–1276.

(37) Zhang, H.; Wang, M. Y. Multi-axis Soft Sensors Based on Dielectric Elastomer. *Soft Robot.* **2016**, *3*, 3–12.

(38) Sadeghi, A.; Mondini, A.; Del Dottore, E.; Mattoli, V.; Beccai, L.; Taccola, S.; Lucarotti, C.; Totaro, M.; Mazzolai, B. A Plant-Inspired Robot With Soft Differential Bending Capabilities. *Bioinspiration Biomimetics* **2016**, *12*, No. 015001.

(39) Sareh, S.; Noh, Y.; Li, M.; Ranzani, T.; Liu, H.; Althoefer, K. Macroband Optical Sensing for Pose Measurement in Soft Robot Arms. *Smart Mater. Struct.* **2015**, *24*, 125024.

(40) Sareh, S.; Jiang, A.; Faragasso, A.; Noh, Y.; Nanayakkara, T.; Dasgupta, P.; Seneviratne, L. D.; Wurdemann, H. A.; Althoefer, K. Bio-Inspired Tactile Sensor Sleeve for Surgical Soft Manipulators. In *2014 IEEE International Conference on Robotics and Automation (ICRA)*, IEEE: 2014; 1454–1459.

(41) Dobrzynski, M. K.; Pericet-Camara, R.; Floreano, D. Contactless Deflection Sensor for Soft Robots. In *2011 IEEE/RSJ International Conference on Intelligent Robots and Systems*; IEEE: 2011; 1913–1918.

(42) Kwon, S.; Kwon, Y.-T.; Kim, Y.-S.; Lim, H.-R.; Mahmood, M.; Yeo, W.-H. Skin-Conformal, Soft Material-Enabled Bioelectronic System With Minimized Motion Artifacts for Reliable Health and Performance Monitoring of Athletes. *Biosens. Bioelectron.* **2020**, *151*, 111981.

(43) Byun, S.-H.; Sim, J. Y.; Zhou, Z.; Lee, J.; Qazi, R.; Walicki, M. C.; Parker, K. E.; Haney, M. P.; Choi, S. H.; Shon, A.; Gereau, G. B.; Bilbily, J.; Li, S.; Liu, Y.; Yeo, W.-H.; McCall, J. G.; Xiao, J.; Jeong, J.-W. Mechanically Transformative Electronics, Sensors, and Implantable Devices. *Sci. Adv.* **2019**, *5*, eaay0418.

(44) Mahmood, M.; Mzurikwao, D.; Kim, Y.-S.; Lee, Y.; Mishra, S.; Herbert, R.; Duarte, A.; Ang, C. S.; Yeo, W.-H. Fully Portable and Wireless Universal Brain–Machine Interfaces Enabled by Flexible Scalp Electronics and Deep Learning Algorithmic. *Nat. Mach. Intell.* **2019**, *1*, 412–422.

(45) Amjadi, M.; Pichitpajongkit, A.; Lee, S.; Ryu, S.; Park, I. Highly Stretchable and Sensitive Strain Sensor Based on Silver Nanowire–Elastomer Nanocomposite. *ACS Nano* **2014**, *8*, 5154–5163.

(46) Cheng, Y.; Wang, R.; Sun, J.; Gao, L. A Stretchable and Highly Sensitive Graphene-Based Fiber for Sensing Tensile Strain, Bending, and Torsion. *Adv. Mat.* **2015**, *27*, 7365–7371.

- (47) Chong, H.; Lou, J.; Bogie, K. M.; Zorman, C. A.; Majerus, S. J. Vascular Pressure–Flow Measurement Using CB-PDMS Flexible Strain Sensor. *IEEE Trans. Biomed. Circuits Syst.* **2019**, *13*, 1451–1461.
- (48) Jeong, Y. R.; Kim, J.; Xie, Z.; Xue, Y.; Won, S. M.; Lee, G.; Jin, S. W.; Hong, S. Y.; Feng, X.; Huang, Y.; Rogers, J. A.; Ha, J. H. A Skin-Attachable, Stretchable Integrated System Based on Liquid GaInSn for Wireless Human Motion Monitoring With Multi-Site Sensing Capabilities. *NPG Asia Mater.* **2017**, *9*, e443–e443.
- (49) Gao, Y.; Li, Q.; Wu, R.; Sha, J.; Lu, Y.; Xuan, F. Laser Direct Writing of Ultrahigh Sensitive SiC-Based Strain Sensor Arrays on Elastomer Toward Electronic Skins. *Adv. Funct. Mater.* **2019**, *29*, 1806786.
- (50) Tang, W.; Yan, T.; Wang, F.; Yang, J.; Wu, J.; Wang, J.; Yue, T.; Li, Z. Rapid Fabrication of Wearable Carbon Nanotube/Graphene Strain Sensor for Real-Time Monitoring of Plant Growth. *Carbon* **2019**, *147*, 295–302.
- (51) Chen, J.; Zhu, Y.; Jiang, W. A Stretchable and Transparent Strain Sensor Based on Sandwich-Like PDMS/CNTs/PDMS Composite Containing an Ultrathin Conductive CNT Layer. *Compos. Sci. Technol.* **2020**, *186*, 107938.
- (52) Wang, X.; Li, J.; Song, H.; Huang, H.; Gou, J. Highly Stretchable and Wearable Strain Sensor Based on Printable Carbon Nanotube Layers/Polydimethylsiloxane Composites With Adjustable Sensitivity. *ACS Appl. Mater. Interfaces* **2018**, *10*, 7371–7380.
- (53) Gogurla, N.; Roy, B.; Park, J.-Y.; Kim, S. Skin-Contact Actuated Single-Electrode Protein Triboelectric Nanogenerator and Strain Sensor for Biomechanical Energy Harvesting and Motion Sensing. *Nano Energy* **2019**, *62*, 674–681.
- (54) Yan, T.; Wang, Z.; Pan, Z.-J. Flexible Strain Sensors Fabricated Using Carbon-Based Nanomaterials: A Review. *Curr. Opin. Solid State Mater. Sci.* **2018**, *22*, 213–228.
- (55) Qiu, A.; Li, P.; Yang, Z.; Yao, Y.; Lee, I.; Ma, J. A Path Beyond Metal and Silicon: Polymer/Nanomaterial Composites for Stretchable Strain Sensors. *Adv. Funct. Mater.* **2019**, *29*, 1806306.
- (56) Lu, N.; Lu, C.; Yang, S.; Rogers, J. Highly Sensitive Skin-Mountable Strain Gauges Based Entirely on Elastomers. *Adv. Funct. Mater.* **2012**, *22*, 4044–4050.
- (57) Pang, C.; Lee, C.; Suh, K.-Y. Recent Advances in Flexible Sensors for Wearable and Implantable Devices. *J. Appl. Polym. Sci.* **2013**, *130*, 1429–1441.
- (58) Cai, L.; Song, L.; Luan, P.; Zhang, Q.; Zhang, N.; Gao, Q.; Zhao, D.; Zhang, X.; Tu, M.; Yang, F.; Zhou, W.; Fan, Q.; Luo, J.; Zhou, W.; Ajayan, P. M.; Xie, S. Super-Stretchable, Transparent Carbon Nanotube-Based Capacitive Strain Sensors for Human Motion Detection. *Sci. Rep.* **2013**, *3*, 1–9.
- (59) Xiao, X.; Yuan, L.; Zhong, J.; Ding, T.; Liu, Y.; Cai, Z.; Rong, Y.; Han, H.; Zhou, J.; Wang, Z. L. High-Strain Sensors Based on ZnO Nanowire/Polystyrene Hybridized Flexible Films. *Adv. Mater.* **2011**, *23*, 5440–5444.
- (60) Amjadi, M.; Yoon, Y. J.; Park, I. Ultra-Stretchable and Skin-Mountable Strain Sensors Using Carbon Nanotubes–Ecoflex Nanocomposites. *Nanotechnology* **2015**, *26*, 375501.
- (61) Mishra, S.; Lee, Y.; Lee, D. S.; Yeo, W.-H. Fractal-Structured, Wearable Soft Sensors for Control of a Robotic Wheelchair via Electrooculograms. In *2017 IEEE 67th Electronic Components and Technology Conference (ECTC)*; IEEE: 2017; 212–217.
- (62) Fan, J. A.; Yeo, W.-H.; Su, Y.; Hattori, Y.; Lee, W.; Jung, S.-Y.; Zhang, Y.; Liu, Z.; Cheng, H.; Falgout, L.; Bajema, M.; Coleman, T.; Gregoire, D.; Larsen, R. J.; Huang, Y.; Rogers, J. A. Fractal Design Concepts for Stretchable Electronics. *Nat. Comm.* **2014**, *5*, 3266.
- (63) Kim, Y.-S.; Mahmood, M.; Lee, Y.; Kim, N. K.; Kwon, S.; Herbert, R.; Kim, D.; Cho, H. C.; Yeo, W.-H. All-in-One, Wireless, Stretchable Hybrid Electronics for Smart, Connected, and Ambulatory Physiological Monitoring. *Adv. Sci.* **2019**, *6*, 1900939.
- (64) Lim, H.-R.; Kim, H. S.; Qazi, R.; Kwon, Y.-T.; Jeong, J.-W.; Yeo, W.-H. Advanced Soft Materials, Sensor Integrations, and Applications of Wearable Flexible Hybrid Electronics in Healthcare, Energy, and Environment. *Adv. Mater.* **2020**, *32*, 1901924.
- (65) Herbert, R.; Kim, J.-H.; Kim, Y. S.; Lee, H. M.; Yeo, W.-H. Soft Material-Enabled, Flexible Hybrid Electronics for Medicine, Healthcare, and Human-Machine Interfaces. *Materials* **2018**, *11*, 187.
- (66) Li, T.; Li, J.; Zhong, A.; Han, F.; Sun, R.; Wong, C.-P.; Niu, F.; Zhang, G.; Jin, Y. A Flexible Strain Sensor Based on CNTs/PDMS Microspheres for Human Motion Detection. *Sens. Actuators, A* **2020**, *306*, 111959.
- (67) Lu, S.; Ma, J.; Ma, K.; Wang, X.; Wang, S.; Yang, X.; Tang, H. Highly Sensitive Graphene Platelets and Multi-Walled Carbon Nanotube-Based Flexible Strain Sensor for Monitoring Human Joint Bending. *Appl. Phys. A: Mater. Sci. Process.* **2019**, *125*, 471.
- (68) Park, J. W.; Kim, T.; Kim, D.; Hong, Y.; Gong, H. S. Measurement of Finger Joint Angle Using Stretchable Carbon Nanotube Strain Sensor. *PLoS One* **2019**, *14*, No. e0225164.
- (69) Wang, L.; Chen, Y.; Lin, L.; Wang, H.; Huang, X.; Xue, H.; Gao, J. Highly Stretchable, Anti-Corrosive and Wearable Strain Sensors Based on the PDMS/CNTs Decorated Elastomer Nanofiber Composite. *Chem. Eng. J.* **2019**, *362*, 89–98.
- (70) Fu, X.; Ramos, M.; Al-Jumaily, A. M.; Meshkinzar, A.; Huang, X. Stretchable Strain Sensor Facilely Fabricated Based on Multi-Wall Carbon Nanotube Composites With Excellent Performance. *J. Mater. Sci.* **2019**, *54*, 2170–2180.
- (71) Ogden, R. W.; Saccomandi, G.; Sgura, I. Fitting Hyperelastic Models to Experimental Data. *Comput. Mech.* **2004**, *34*, 484–502.
- (72) Trueman, E. R. *The Locomotion of Soft-Bodied Animals*; Edward Arnold: 1975.
- (73) Galloway, K. C.; Polygerinos, P.; Walsh, C. J.; Wood, R. J. Mechanically Programmable Bend Radius for Fiber-Reinforced Soft Actuators. In *2013, 16th International Conference on Advanced Robotics (ICAR)*; IEEE: 2013; 1–6.